Original article

Nanocrystalline NiTiB reinforced aluminum matrix composites: Synthesis, structural, mechanical and corrosion properties

Muharrem Pul[1] (iD), İlker Emin Dağ[2], Tuncay Şimşek[3] (iD),
Barış Avar[2] and Arun K. Chattopadhyay[4]

Abstract

In this study, aluminum composites were developed using a powder metallurgy route by incorporating varying amounts of nanocrystalline NiTiB into the Al2024 alloy. The effects of nanocrystalline NiTiB on the structural, morphological, corrosion, and mechanical properties of the aluminum composites were thoroughly investigated. The results showed that the base alloy and composites with 2% and 4% NiTiB exhibited the highest relative density. The composite with 4% NiTiB achieved the maximum hardness of 87.4 HV. Additionally, the inclusion of nanocrystalline NiTiB significantly improved the compressive strength, corrosion resistance, and wear resistance of the composites. Specifically, the compressive strength increased by approximately 2% with 2% NiTiB and by around 13% with 12% NiTiB. Corrosion resistance was highest in the composite with 4% NiTiB, as confirmed by electrochemical impedance spectroscopy. In the wear-loss study, the wear loss of the composites was found to be reduced by 244% and 457% for those reinforced with 2% and 12% NiTiB, respectively. These findings underscore the potential of nanocrystalline NiTiB to enhance the performance of Al2024 composites in applications demanding superior corrosion resistance, mechanical strength, and wear resistance.

Introduction

Composite materials are categorized into polymer matrix composites, metal matrix composites (MMCs), and ceramic composites based on the structure of the matrix phase.[1] Metal matrix composites consist of a ductile metal matrix and dispersed particles, fibers, whiskers, or nanomaterials.[2] MMCs find extensive applications in aerospace, automotive, defense, and other fields. Silicon Carbide (SiC), Titanium Dioxide (TiO_2), Aluminum Oxide (Al_2O_3), Boron Carbide (B_4C), Yttrium Oxide (Y_2O_3), Silicon Nitride (Si_3N_4), and Aluminum Nitride (AlN) are commonly used reinforcements in MMCs.[3] Among MMCs, pure and alloyed aluminum are extensively studied as matrix materials due to their low density, corrosion resistance, precipitation strengthening, vibration damping, and thermal/electrical conductivity. Aluminum matrix composites possess various mechanical properties, making them suitable for a wide range of applications.[4]

Recent studies have extensively researched several surface treatment methods aimed at enhancing wear resistance, corrosion resistance, and mechanical properties. Among the materials studied, Ti–Ni-B alloys have garnered significant attention due to their exceptional properties, which include high strength, ductility, corrosion resistance, and biocompatibility. These characteristics make Ti–Ni-B alloys highly suitable for practical applications, especially given their excellent shape memory effect characteristics.[5,6] One notable method

[1]Department of Electirical and Energy, Kırıkkale Vocational School, Kırıkkale University, 71450 Kırıkkale, Turkey
[2]Department of Metallurgical and Materials Engineering, Zonguldak Bülent Ecevit University, 67100 Zonguldak, Turkey
[3]Department of Mechanical and Metal Technologies, Kırıkkale University, 71450 Kırıkkale, Turkey
[4]AMAERO Inc., 130 Innovation Drive, McDonald, Tennessee, 36353, USA

Corresponding author:
Muharrem Pul, Department of Electirical and Energy, Kırıkkale Vocational School, Kırıkkale University, Kırıkkale 71450, Turkey.
Email: mpul@kku.edu.tr

involves the diffusion of boron atoms into the substrate material to form hard boride layers. Boron atoms, due to their relatively small radii, can easily diffuse into the substrate material, enhancing the hardness and wear resistance of the treated surface. This method has shown promise in improving the surface properties of various materials.[7,8]

In the context of medical implants, bulk and porous nitinol (NiTi) alloys stand out as a promising class due to their high corrosion resistance and deformation behavior that closely mimics the bone tissues of the human body. Nitinol's unique properties make it an excellent candidate for use in biomedical applications, particularly in implants that need to withstand harsh conditions within the human body while maintaining their structural integrity.[9] Aluminum alloying of nitinol has emerged as a convenient tool for controlling both corrosion and mechanical properties. Studies on nitinol alloyed with aluminum have been conducted using various methods, including casting, additive manufacturing, and powder metallurgy. The alloying process leads to the formation of various nickel and titanium aluminides. It revealed the presence of multiple ternary compounds, such as $Al_{13}Ni_2Ti_5$, Al_2NiTi, Al_3NiTi_2, and $AlNi_2Ti$. Monolithic NiTi alloyed with 6–9 atomic percent (at %) aluminum demonstrates significantly increased ultimate compressive strength and martensitic shear stress. The favorable effects of aluminum alloying on the bulk nitinol strength can be attributed to the solid solution hardening of the B2 phase with aluminum atoms. Depending on the composition and temperature, numerous chemical reactions between the components have been studied, providing a deeper understanding of the material's behavior under various conditions. The sintering mechanisms of the TiNiAl system have been thoroughly investigated using techniques such as X-ray diffraction, elemental analysis, differential thermal analysis, and electron microscopy. These studies revealed that the obtained NiTi alloy consists of the TiNi, Ti2Ni, and AlNi2Ti phases, contributing to the overall improvement in the material's mechanical and corrosion resistance properties.[6,10]

The 2024 aluminum alloy, part of the Al-Cu-Mg series, is high-strength duralumin with a finely distributed second phase. Its excellent plasticity makes it ideal for high-load components like aircraft skins, spars, and ribs. Widely used in civil and military aviation, it is indispensable in the industry despite its limited corrosion resistance.[11] This alloy is known for its excellent strength-to-weight ratio and is commonly used in aerospace applications. Al2024 alloy exhibits good strength, workability, and high fatigue resistance, making it comparable to other aluminum alloys. Its lightweight nature makes it preferred in aircraft components such as wings, pistons, and cylinder heads.[12] Previous studies have explored the properties of Al2024 matrix composites produced using different methods and reinforced with various particles.[13] Murth et al. investigated the effects of granulated blast furnace slag and fly ash on AA2024 composites produced via the stir-casting route.[14] Similarly, Rebba and Ramaniah conducted an experimental study on the mechanical properties of Al2024 composites reinforced with molybdenum powders.[15] Dey and Biswas examined the mechanical and tribological properties of Al2024-SiC and Al2024-TiB$_2$ composites prepared using the stir casting technique.[16] Nuruzzaman et al. explored the effects of aluminum-aluminum oxide (Al-Al$_2$O$_3$) metal matrix composites with varying weight percentages of aluminum oxide reinforcements at different sintering temperatures.[17] Luo and Sun studied the influence of interfacial bonding on the tensile fracture characteristics of boron-fiber-reinforced aluminum (B/Al) composites.[18] Heiadarpour focused on aluminum composites reinforced with the Ti$_2$SC MAX phase, fabricated through friction stir processing.[19] Kumar et al. reported a comparative study of Al-TiB$_2$ composites produced using different powder metallurgical techniques.[20] Recently, the effects of various B$_4$C and TiB reinforcements on Al2024 composites produced by powder metallurgy were detailed.[21]

In this study, the powder metallurgy method was employed to produce composite materials with NiTiB alloy. Powder metallurgy aims to develop high-strength materials with good compactness through blending, compaction, and sintering processes. This study investigates the impact of NiTiB additions on the densification, microstructure, hardness, and corrosion behavior of Al-2024. Going by the literature references, it is expected that the addition of NiTiB would likely impact the densification, microstructure, hardness, and corrosion behavior of Al-2024 alloy and also improve its mechanical, tribological, corrosion, and high-temperature properties. In this study up to 12 wt.% of NiTiB alloy were introduced to optimize and tailor the overall Al2024 composite. In this study, the sintered composites were investigated for densification, microstructural features, and hardness of these composites. Corrosion tests were then conducted on composites with superior density and hardness in 3.5% NaCl solution at room temperature to evaluate their suitability for marine applications. The PM method adopted for this study offers advantages over other production methods for metal matrix composites. One of the main challenges in MMC production is achieving sufficient wetting between the matrix metal and reinforcing particles. Poor wetting results in incomplete encapsulation of reinforcing particles, leading to inadequate bonding at the interface. The powder metallurgy method provides better control of interfacial kinetics and increases the wetting levels at the interface, addressing this challenge.

Materials and methods

Materials

In this study, mechanically alloyed NiTiB nanoparticles were utilized as reinforcement materials. Nickel (Ni), Titanium (Ti), and Boron (B) starting powders were obtained from Aldrich Chemicals with purities of 99.99%, 99.7%, and 99.7%, respectively. The powders were used as-received without further treatment. The ball milling process was carried out for 120 hours in a

planetary ball mill, as previously described by the authors.[5] All experiments involving sample handling and mechanical alloying were conducted under an argon atmosphere. The Al2024 alloy powders were also used as-received as the base matrix for the composite preparation. The chemical composition and properties of the Al2024 alloy are provided in Table 1 and Table 2, respectively.

Production of composites

The composite materials were produced using the powder metallurgy method. Initially, NiTiB nanopowders with weight percentages of 2, 4, 8, and 12 were accurately weighed and mixed with Al2024 powder. The mixing process was performed in a drum mixer with 5 mm diameter zirconia balls at a powder-to-ball weight ratio of 8:1. The mixer was rotated at a speed of 300 rpm for 20 hours. The primary reason for using zirconia balls instead of conventional stainless steel balls in ball milling is their superior hardness, which results in minimal wear and tear. Additionally, zirconia balls prevent ferrous contamination, ensuring a purer milling process.

In the next stage, the composite mixtures were compacted in a steel mold under a pressure of 750 MPa. The resulting samples had a diameter of 16 mm and a length of 20 mm. Finally, the composite samples were subjected to a sintering process in a heat treatment furnace. The sintering was carried out at a constant temperature of 575 °C for a duration of 90 minutes, completing the production process of the composite samples.

Microstructure and phase analysis

XRD analysis was conducted on both the nano NiTiB powders and the NiTiB-reinforced Al2024 composites to investigate potential phase changes resulting from the production process. The XRD measurements utilized Cu-Kα radiation ($k = 1.54$ Å) with an anode voltage of 40 kV and an anode current of 30 mA. Data collection was performed in the 2θ range from 10° to 90°, with a scanning rate of 4°/min. The crystalline phases were

Table 1. Chemical composition of Al 2024 alloy.

Weight	Cu	Mg	Mn	Si	Fe	Zn	Ti	Cr	Al
%	4.00	1.50	0.60	0.50	0.50	0.25	0.15	0.10	Rest

Table 2. Properties of Al20224 alloy.

Density (g/cm³)	2.77
Young's Modules (GPa)	73
Shear Strength (MPa)	285
Strength Weight Ratio (KN-m/Kg)	177
Ultimate Tensile Strength(MPa)	490
Yield Tensile Strength (MPa)	350
Thermal Conductivity (W/m-K)	120
Hardness (Brinell)	120

identified by referring to the International Center for Diffraction Data (ICDD) powder diffraction files.

Furthermore, optical microscope, scanning electron microscope (SEM) analysis, and EDX analysis were conducted to examine the microstructures and elemental composition of the NiTiB-reinforced Al2024 composites. These techniques allowed for the characterization and visualization of the composite's internal structure, as well as the identification of the elemental constituents present in the material.

Density and porosity

The theoretical densities were calculated three times for each sample on a WSA224 balance according to Archimedes' principle using ASTM B962-15 standard and Equation (1).[22]

$$\rho_c = \frac{w}{w - w_t} \times \rho w \tag{1}$$

where ρ_c is the density of the produced sample, ρ_w is the density of pure water, w is the weight of the composite in air and w_t is the weight of the composite in water. After the experimental densities were found, the theoretical density of bulk structures varying according to the secondary reinforcement ratio was calculated from the rule of mixtures according to Equation (2).[23]

$$\rho_t = (\rho_m \times wt\%) + (\rho_r \times wt\%) \tag{2}$$

where ρ_m is the theoretical density of the sample and ρ_r is the density of the reinforcement particle.

Porosity values were also calculated from Equation (3). Calculations were made using experimental and theoretical densities.[22]

$$\text{Porosity}(\%) = \frac{\text{Theoretical density} - \text{Experimental density}}{\text{Theoretical density}} \times 100 \tag{3}$$

Hardness tests were performed three times for each sample with Shimadzu HMV-G21 microhardness tester. After each test, the average diagonal size of the traces was found with 400x magnification and calculated according to the Equation (4).

$$HV = 1.8544 F/d^2 \, \text{kg/mm}^2 \tag{4}$$

The HV number is calculated by the ratio F/A, where F represents the force applied to the diamond in kilograms-force, and A is the surface area of the resulting indentation in square millimeters.

$$A = d^2/2\sin\left(\frac{136°}{2}\right) \tag{5}$$

which can be approximated by evaluating the sine term to give,

$$A \approx d^2/1.8544 \tag{6}$$

where d is the average length of the diagonal left by the indenter in millimeters. Hence,

$$HV = F/A = 1.8544 \, F/d^2 \qquad (7)$$

where F is in kgf and d is in millimeters.

The tests were carried out with static load for 15 seconds under 5, 10, and 50 g load. Since the hardness values showed similar values for the secondary particles, only the matrix hardness was calculated.

Corrosion tests

Electrochemical impedance spectroscopy (EIS) and potentiodynamic polarization tests were conducted using a potentiostat/galvanostat (Gamry Interface 1010E Gamry Instruments Inc. 72 Warminster, PA, USA) to evaluate the corrosion resistance of the fabricated composites. The experiments were performed at room temperature (23 ± 2 °C) with an average humidity of $60 \pm 23\%$. Each test was repeated three times to ensure accuracy and reliability. Prior to the tests, the samples underwent polishing using 2500 grit abrasive paper and were subsequently cleaned with ethanol for 5 minutes after mirror polishing with a 1 μm diamond suspension.

The electrochemical experiments were carried out in a polycarbonate test chamber using a 3-electrode system. A graphite rod served as the counter electrode, while a saturated calomel electrode (SCE) was used as the reference electrode. The composite samples served as the working electrode. The exposed surface area of the composites was 0.78 cm² for all electrochemical tests. Before the electrochemical experiments, the composites were immersed in a 3.5% saline solution, simulating the composition of seawater, for 20 minutes to stabilize the open circuit potential (OCP).

The stability of the composites without polarization was evaluated by monitoring the OCP over time. Following 20 minutes of OCP measurement, potentiodynamic polarization tests were conducted at a scan rate of 1 mV/s within the range of ± 0.5 V relative to the OCP. The corrosion potential (E_{corr}), corrosion current (i_{corr}), Anodic Tafel Slope (βa), and Cathodic Tafel Slope (βc) values were obtained from the resulting polarization curves. The corrosion rate was calculated according to the ASTMG102 standard using Equation (8), where E_{corr} represents the corrosion potential (V), i_{corr} is the corrosion current density (μA/cm²), EW denotes the equivalent weight, ρ represents the density, K1 is a constant value for mm/year, and CR corresponds to the corrosion rate.[24]

$$CR = K1 i_{corr} \frac{EW}{\rho} \qquad (8)$$

Polarization resistance was also calculated according to the Stern Geary equation as given in Equation (9).[25] Here i_{corr} is the corrosion current density (A/cm²), Rp is

the polarization resistance (ohms.cm²), ßa and ßc are the anodic and cathodic Tafel slope (volts/decade).

$$i_{corr} = \frac{1}{2.303 Rp} \left(\frac{\text{ß}a x \text{ß}c}{\text{ß}a + \text{ß}c} \right) \qquad (9)$$

To ensure consistent testing conditions and stabilize the samples, all samples were subjected to sanding with 2500 grit sandpaper and polishing with a 1 micrometer solution after the potentiodynamic polarization tests. This step aimed to restore the surface condition and remove any potential artifacts resulting from the polarization tests.

To maintain test consistency and allow for sample stabilization, the samples were immersed in a 3.5% solution for 20 minutes before conducting the electrochemical impedance spectroscopy (EIS) tests. EIS tests were performed using a sinusoidal wave intensity of 10 mV within the frequency range of 0. 2 Hz to 100 kHz. The EIS technique is a nondestructive method that provides valuable information about the corrosion behavior of materials. However, it is important to standardize the testing conditions and minimize potential influences from previous tests to ensure accurate and reliable results.

To determine the mechanical values of composite materials, hardness measurements, pressure tests, and abrasive wear tests were carried out. Mechanical tests and measurements were carried out in an open atmosphere under normal conditions. The methods and parameters of the mechanical tests performed are given separately in the "Results and Discussion" section.

Results and discussion

XRD analysis

The XRD analysis of the mechanically alloyed NiTiB nanoparticles after 120 hours of milling revealed the presence of $Ni_{21}Ti_2B_6$ phases, indicating successful synthesis without impurities. However, some amorphization was observed due to the plastic deformations during the milling process. Mechanical alloying involves cold welding, flattening, and fracturing of the starting powders, resulting in deformation hardening and reduction in crystallite size.[26] The crystallite size and lattice strain of the milled powders were calculated using the Williamson-Hall Equation, yielding values of 5.8 nm and 1.521%, respectively.

It is known that increased milling time leads to both powder particle refinement and grain refinement. Consequently, nanometer-sized particles are achieved with prolonged milling periods. Depending on the material and processing conditions, crystallite sizes typically range from 5 to 50 nm. This refinement enhances the material's properties, making it more suitable for various advanced applications. Additionally, extended milling can improve the uniformity and distribution of the particle sizes, contributing to the overall consistency of the final product.[27]
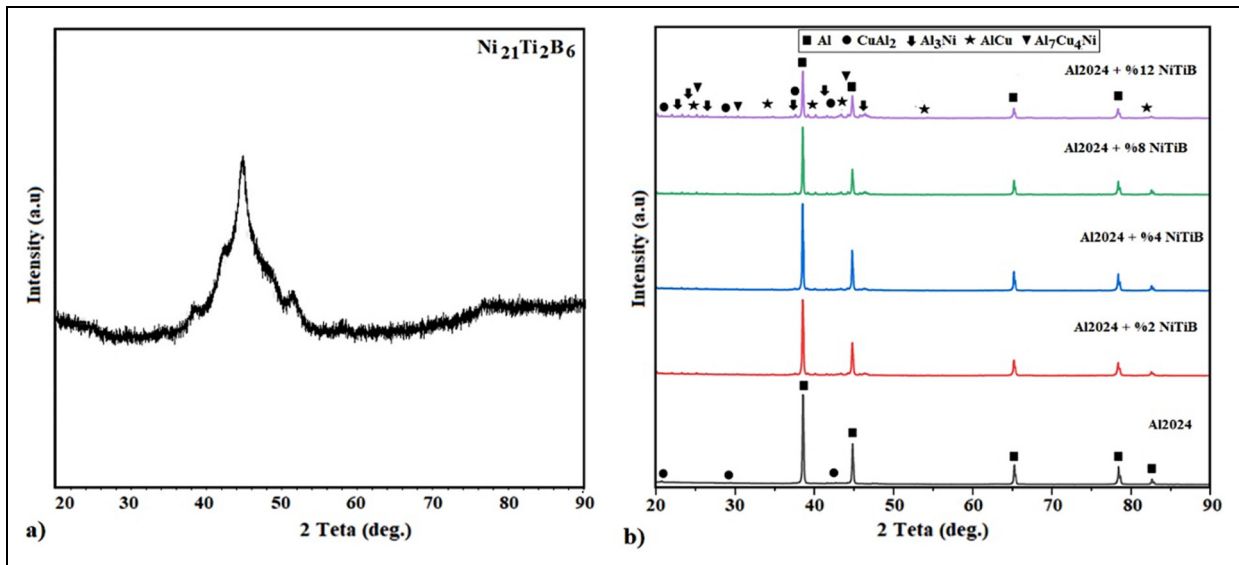
Figure 1. XRD patterns of the (a) Reinforcement nano NiTiB powder, (b) Unreinforced Al2024 matrix and Composite samples.

The XRD patterns of the as-sintered Al2024 matrix and the nano NiTiB-reinforced composites were also analyzed. The unreinforced Al2024 samples exhibited peaks corresponding to the Al and $CuAl_2$ phases, consistent with previous studies. The XRD patterns of the composites showed the presence of Al_3Ni, AlCu, Al_7Cu_4Ni, as well as Al and Al_2Cu phases. With increasing amounts of reinforcement powders, the peaks corresponding to Al_3Ni, AlCu, and Al_7Cu_4Ni became sharper, indicating improved crystallinity. In contrast, the peak intensities and broadening of the Al and Al_2Cu phases decreased as the NiTiB content increased. These findings suggest the successful incorporation of nano NiTiB reinforcement into the Al2024 matrix, leading to structural modifications in the composite materials.

Microstructural observations

The SEM images of the nano NiTiB powders are shown in Figure 2, displaying a homogeneous and uniformly distributed NiTiB phase. The particle morphologies mainly exhibited spherical shapes, with some irregular shapes within the particle size distribution of 5–70 μm. As expected, long milling times of around 120 hours have significantly reduced the sizes of the initial powders. The powders obtained at the end of milling do not show significant differences due to deformation hardening and exhibit similar morphological structures.[27] The EDX images further confirmed the formation of NiTiB without any impurities.

To investigate the microstructures of Al2024/NiTiB composite materials, both optical and SEM studies were conducted to capture images at different magnifications. Firstly, SEM pictures with 500 × magnification, as shown in Figure 3, were taken to examine the distribution of NiTiB reinforcement particles within the Al2024 matrix.

The SEM images in Figure 3 show that the NiTiB nanocrystalline particles appear brighter within the composite structures. As the NiTiB content increases in the composites, a more homogeneous distribution of NiTiB is achieved. However, there is also evidence of localized agglomeration of the reinforcement with higher NiTiB content in the aluminum matrix. This agglomeration phenomenon is commonly observed in particle-reinforced metallic composites and has been reported in previous studies.[28] It is worth noting that the agglomeration of NiTiB particles in the composite structure contributes to increased void formation. Similar observations have been reported in the literature.[29] Furthermore, an increase in the particle reinforcement content within the composite structure leads to an increase in porosity. These findings highlight the structural characteristics and behavior of the NiTiB-reinforced composites, emphasizing the need for careful control of the reinforcement content to minimize agglomeration and porosity for optimal composite performance.[30,31]

Considering the homogeneous distribution of the reinforcement materials within particle-reinforced metallic composites, the powder metallurgy technique is generally acknowledged to be more advantageous compared to other methods, as supported by existing literature.[32,33] To assess the presence and distribution of structural elements within the composite, EDX analysis was performed, and the SEM elemental mapping images showing the distribution of elements within the structure are presented in Figure 4. These images provide valuable insights into the spatial arrangement and dispersion of different elements within the composite.

Upon examining the EDX analysis and SEM mapping images in Figure 4, it is evident that the primary alloying element copper (Cu) of the matrix material Al2024 and the important alloying element magnesium (Mg) are detected within the structure. Additionally, the elemental
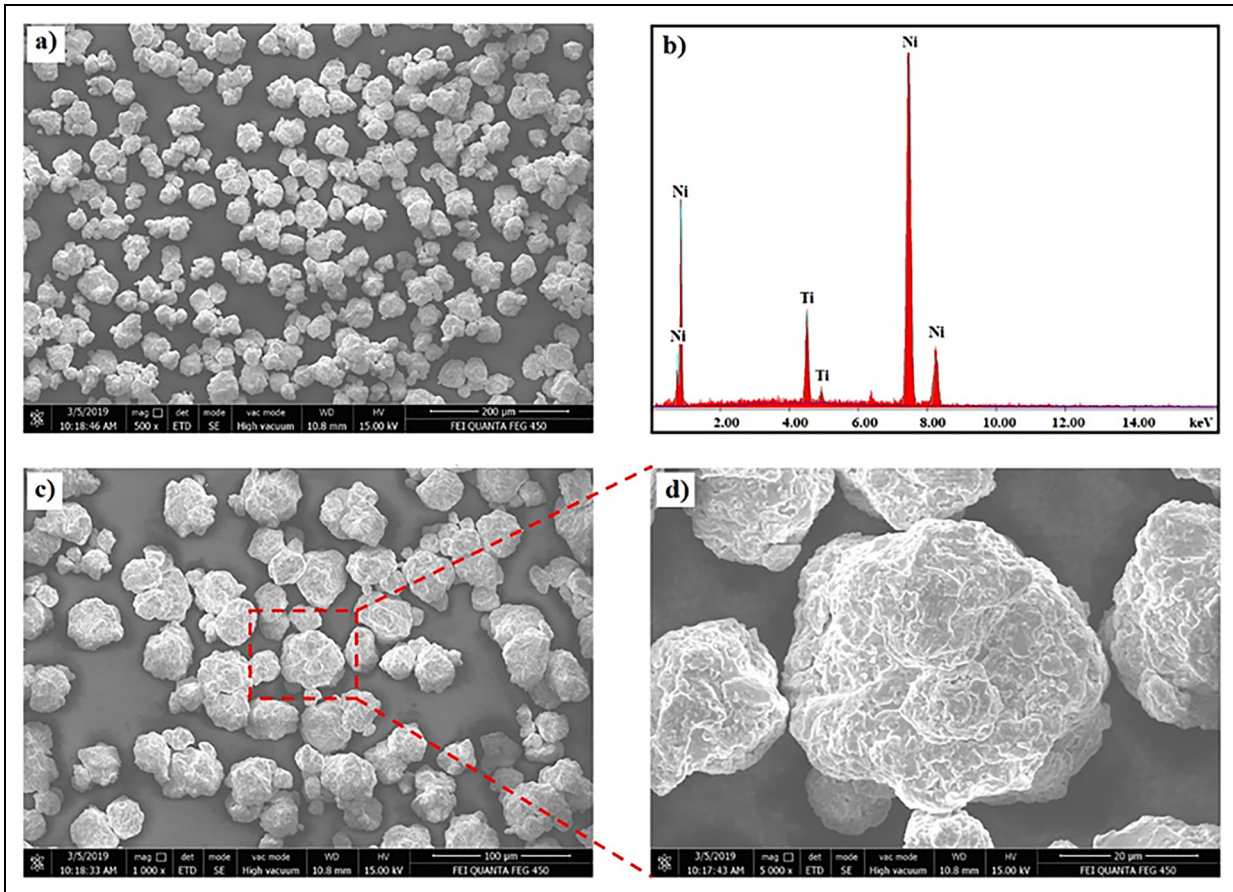
Figure 2. SEM and EDX images of the nano NiTiB powders.

composition corresponding to the nanocrystalline NiTiB reinforcement is also clearly identified. However, due to the atomic structure characteristics, the detection of boron (B) is not sufficient with these analyses.

The sintering temperature of 575°C and sintering time of 90 minutes employed in the powder metallurgy production process are found to be adequate based on a detailed analysis of the composite structure. The SEM images in Figure 3 indicate the absence of porosity at the interfaces between the Al2024 matrix and the NiTiB reinforcement, suggesting favorable wetting between the two materials. To further investigate the matrix-reinforcement interface and assess the effect of sintering on the Al2024 matrix, additional SEM images in Figure 5 are presented.

It is to be noted in this context that it is unlikely to have any other possible reactions between NiTiB and Al2024 during sintering at 575 °C. The reason is that sintering typically involves heating a material below its melting point to promote densification and bonding between particles. At this temperature range, the individual alloy components are not expected to undergo significant chemical reactions with each other.

Upon close examination of the SEM images presented in Figure 5, it is evident that the Al2024 matrix material and the NiTiB nanocrystalline reinforcement exhibit satisfactory wetting, with no apparent porosity formation at the matrix-reinforcement interfaces. However, occasional small voids are observed between the Al2024 particles. The interfacial lines between the Al2024 particles indicate significant neck and bond formation. To mitigate the presence of these minimal voids, it is suggested that future studies consider increasing the sintering temperature and/or duration to enhance the elimination of these voids.

Mechanical properties

Density and hardness measurements. The presence of porosity has a significant influence on mechanical properties such as hardness and wear resistance. Figures 6 and 7 illustrates the experimental density, theoretical density, and relative density values of the composites. It can be observed that the theoretical density increases with higher particle reinforcement due to the higher density of the NiTiB particles, as shown in Figure 7. The experimental density for the undoped Al2024 sample was determined as 2. 23 g/cm^3, while it increased to 2. 38 g/cm^3 and 2. 41 g/cm^3 for the 2% and 4% doped samples, respectively. However, despite the higher secondary particle content, the densities were measured as 2. 42 g/cm^3 and 2. 44 g/cm^3 for the 8% and 12% doped samples, respectively, due to low cohesion.

These results indicate that the addition of NiTiB initially enhances the coalescence rate of aluminum grains. However, as the agglomeration effect and the proportion
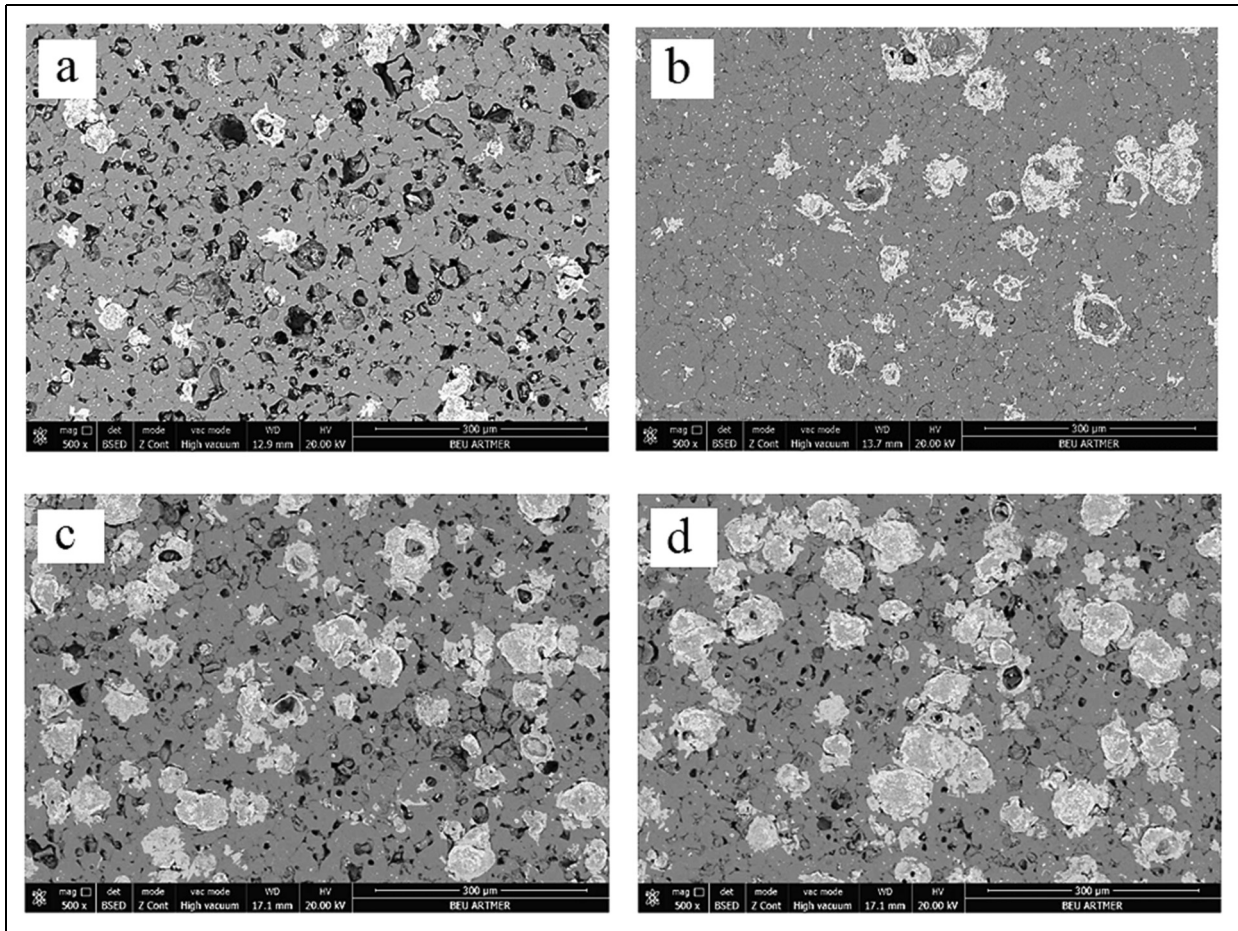
Figure 3. Al2024/NiTiB composite structures reinforced with (a) 2%, (b) %4, (c) %8, (d) %12 NiTiB.

of hard particles increase, the porosity value also increases due to the difficulty of achieving a strong bond with the aluminum matrix.[34]

Table 3 presents the matrix microhardness values obtained under static loads of 5, 10, and 50 g. The influence of the NiTiB particle content and porosity on the hardness is evident. Particularly, in the 2% and 4% doped samples with high theoretical density, the hardness values increased significantly from 47.12 HV to 66.3 HV and 84.1 HV, respectively, under a 5 g load. This can be attributed to the deformation-hardening effect of the NiTiB particles. Similar increases in hardness were observed for the 10 g and 50 g loads.[35] However, as the NiTiB content increased, agglomeration occurred, hindering the coalescence of the Al2024 grains under pressure and resulting in lower density. Consequently, the matrix exhibited altered behavior against loads, leading to a decrease in hardness.

Compressive strength. Compression tests were performed on NiTiB fiber-reinforced composite structures using a hydraulic compression machine at a loading rate of 2400 N/s to determine their compressive strength values. The obtained values are presented in Table 4 and the graph constructed based on these values is shown in Figure 8.

The graph clearly indicates that the addition of NiTiB reinforcement initially enhances the compressive strength of the composite materials. Compared to the pure Al2024 matrix, the specimen reinforced with 2% NiTiB exhibits a 2% increase in compressive strength, while the specimen reinforced with 12% NiTiB shows a significant 13% increase. This improvement in strength can be attributed to various strengthening mechanisms in particle-reinforced composites.

During the sintering heat treatment process, the Al2024 matrix and NiTiB reinforcement materials exhibit different thermal expansion behaviors. This significant difference in thermal expansion creates dislocations at the interfaces, resembling particle pinning. The smaller grain size and higher hardness of the reinforcing particles lead to an increase in dislocation density, thereby enhancing the mechanical strength of the composite. These findings align with similar results reported in the literature.[36]

Furthermore, the successful bonding between the matrix and reinforcement, as observed in the microstructure analysis, plays a crucial role in determining the mechanical strength of the composite. The strength of the interfacial bonding directly influences the overall mechanical strength of the composite. Therefore, the presence of strong interfacial bonding, as supported by the obtained compressive strength values, reinforces the proposition made earlier.
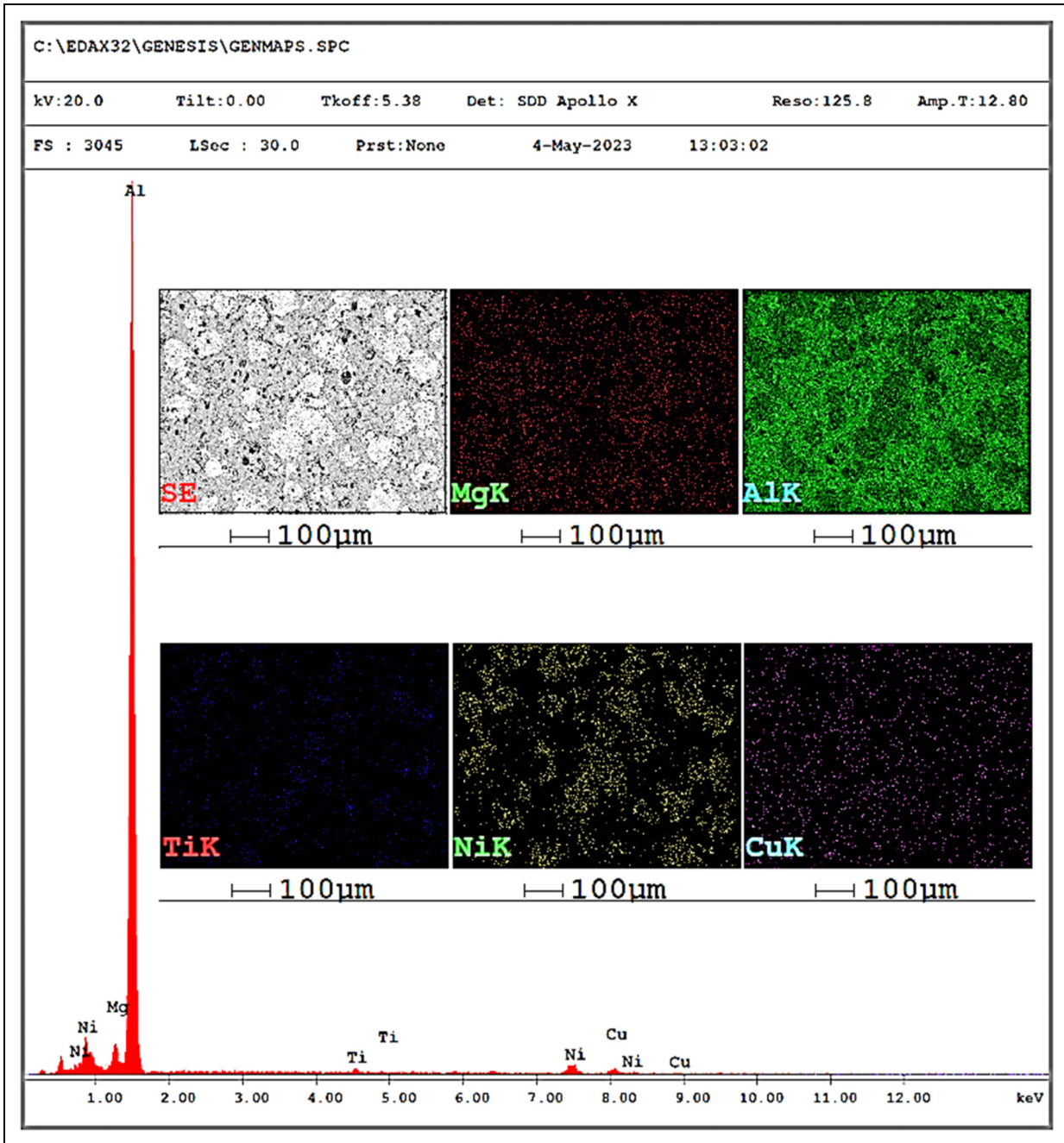
Figure 4. EDX analysis and elemental distribution of Al2024/NiTiB composite structure.

In conclusion, the addition of NiTiB reinforcement not only enhances the mechanical strength of the composites but also highlights the importance of interfacial bonding for achieving optimal mechanical performance.

Corrosion behavior

Figure 9 shows the open circuit potential curves of Al2024/NiTiB composites measured in 3.5% NaCl solution for 1200 seconds as a function of time. OCP measurements are a simple way to monitor corrosion behavior in a system. OCP measures the resting potential between a working electrode and the environment relative to a reference electrode. High OCPs indicate a system is more likely to undergo reduction, as it takes up electrons instead of losing them. Conversely, a dropping OCP signifies oxidation and the accumulation of negative charges. Long-term OCP changes reflect shifts in the corrosion system due to alterations in anodic and cathodic reactions. The more positive values of the open circuit potential are associated with higher corrosion resistance.[37] As shown in Figure 9, the Al2024 pellet with the lowest corrosion potential has the lowest corrosion resistance in a 3.5% NaCl solution. In addition, the OCP values of Al2024 and 2% NiTiB added composites showed a continuous trend towards a more negative value within 20 minutes. This is due to the penetration of the corrosive environment on the surface of these materials and the inability of
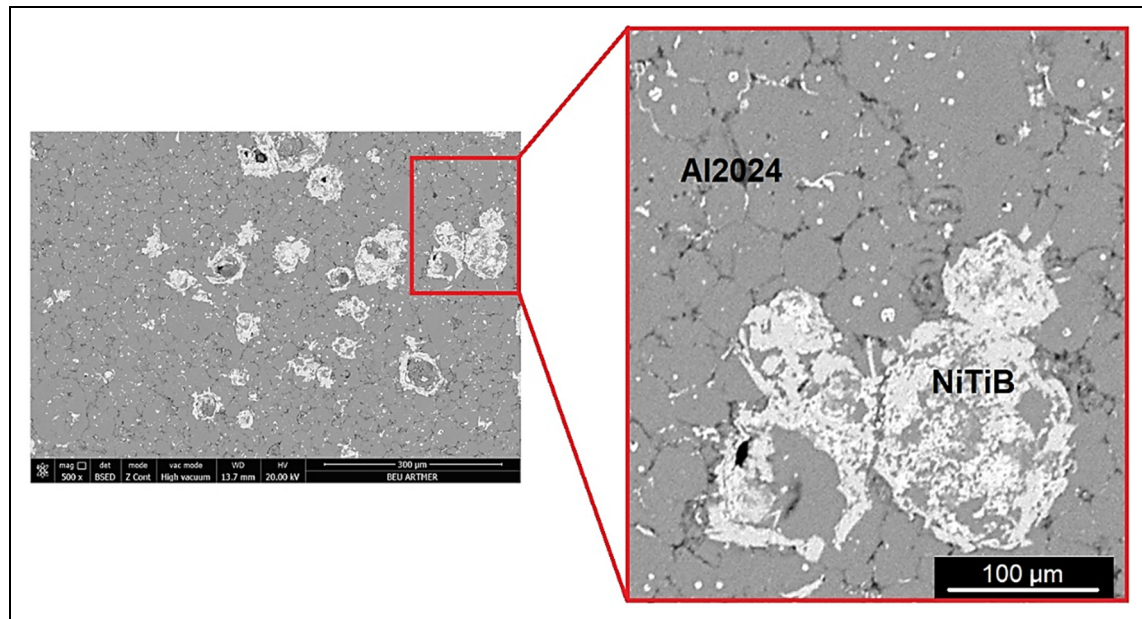
**Figure 5.** Detailed view of the matrix-reinforcement interface surface.
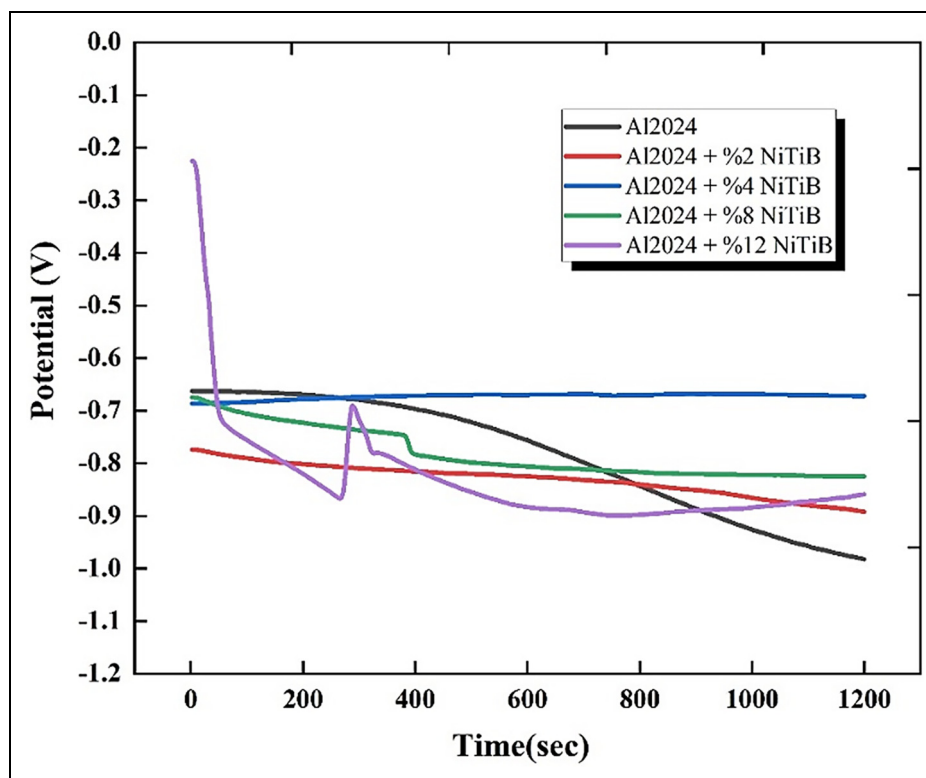
Figure 6. Relative density values of the Al2024/NiTiB nanocomposites with different amounts of NiTiB.

corrosive layers such as Al_2O_3 and TiO_2 to provide sufficient protective effect.[38]

The OCPs of the composites containing 4%, 8%, and 12% NiTiB exhibit higher values compared to Al2024 and Al2024 + 2%NiTiB composition. The abrupt decrease in potential observed in the 8% and 12% reinforced samples can be attributed to the corrosive behavior resulting from the inhomogeneity of the composites and the gaps between the domains of aluminum and NiTiB. In the 12% NiTiB sample, the reduction behavior initially falls sharply, then temporarily recovers, and subsequently declines again until it reaches a steady value. These erratic trends indicate inconsistencies within the composite matrices. However, these composites demonstrate stable behavior after 500 seconds, indicating an increase in passivation.[39] The SEM photograph in Figure 9 confirms that
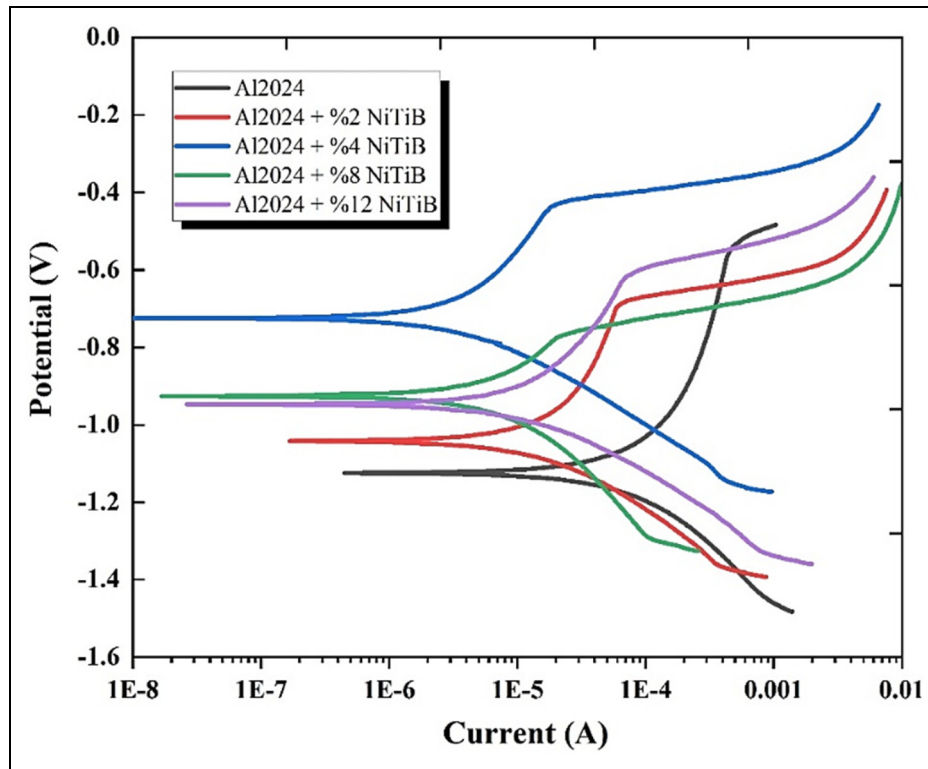
Figure 7. Theoretical and experimental density values of the Al2024/NiTiB nanocomposites with different amounts of NiTiB.

Table 3. Vickers microhardness values of the Al2024/NiTiB composites.

Sample	HV0.005	HV0.01	HV0.05
Al2024	47.12	41.15	38.23
Al2024 + %2 NiTiB	66.3	66.2	54.8
Al2024 + %4 NiTiB	84.1	87.4	66.7
Al2024 + %8 NiTiB	57.8	59.1	56.2
Al2024 + %12 NiTiB	43.3	42.5	42.7

Table 4. Compressive strength values of the Al2024/NiTiB composites.

| Sample	Compressive strength (N/mm^2)
Al2024	266,0000
Al2024 + %2 NiTiB	271,2000
Al2024 + %4 NiTiB	283,3000
Al2024 + %8 NiTiB	296,9000
Al2024 + %12 NiTiB	301,2000

the NiTiB particles exhibit optimal bonding behavior with the Al2024 surface in the 4% reinforced sample, contributing to its high passivation behavior. This sample also exhibits the highest corrosion resistance in a stable solution, as evidenced by its highest open circuit potential. The higher corrosion potential compared to the 8% and 12% reinforced samples can be attributed to the secondary particles, which are less agglomerated and more homogeneously distributed, thus minimizing micro-galvanic

effects.[40] Figure 10 illustrates the potentiodynamic polarization curves of the Al2024 alloy and NiTiB-doped samples, and the corresponding values calculated from the anodic and cathodic polarization curves are presented in Table 3. Higher corrosion potential (Ecorr) and polarization resistance (Rp) indicate greater corrosion resistance, while lower corrosion current density indicates higher corrosion resistance.[41] From Figure 10 and Table 5, it can be observed that the pure Al2024 alloy exhibits the lowest Ecorr value of −1. 128 V and the highest icorr value of 88.44 μA/cm^2, indicating the lowest corrosion resistance. Similarly, the Rp value is also the lowest for the pure Al2024 alloy. This suggests that the incorporation of TiB$_2$ reinforcement into the aluminum alloy reduces the corrosion rate by promoting the formation of a protective passive film.[41] Additionally, TiB$_2$ provides good adhesion to the grain boundaries, reducing defect formation and preventing intergranular corrosion.[42]

While examining Table 5 and Figure 10, it is evident that the 4% NiTiB-doped sample exhibits the lowest corrosion rate and the highest corrosion resistance. The SEM photograph in Fig. 3 reveals a more homogeneous distribution of NiTiB particles in the 4% doped sample. This homogeneous distribution prevents the breakdown of the passive film by filling the gaps between the particles. On the other hand, with an increase in the NiTiB content, agglomeration occurs, leading to a decrease in corrosion potential, an increase in corrosion current density, and a gradual decrease in polarization resistance due to micro-galvanic effects.[40,41] However, despite the reduction in
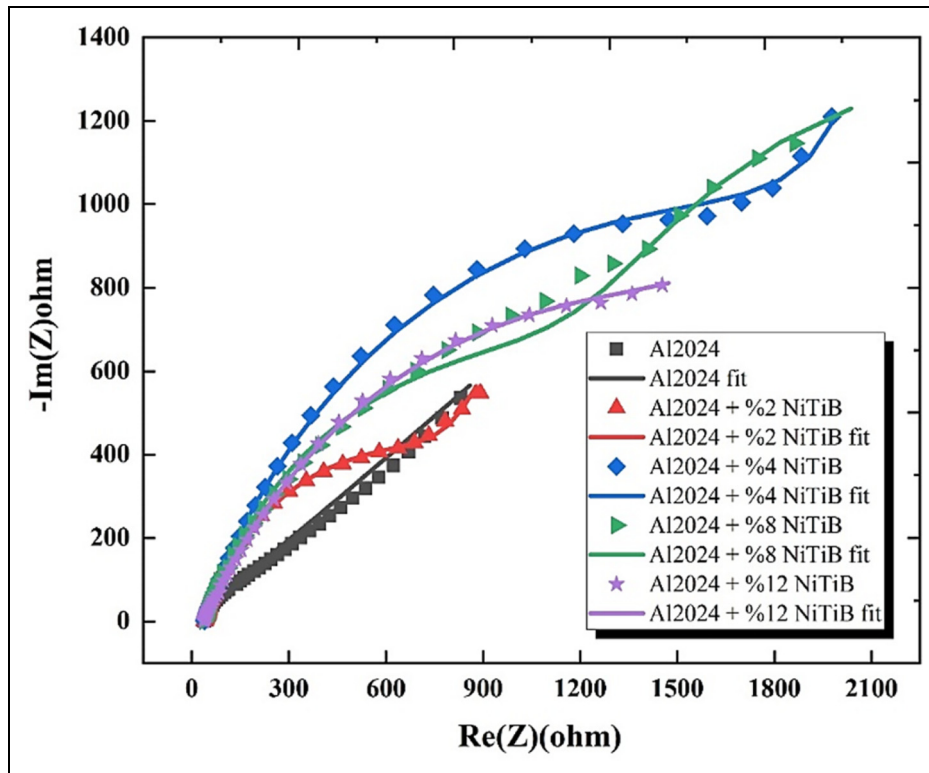
Figure 8. Compressive strength values of Al2024/NiTiB nanocomposites containing different amounts of NiTiB.
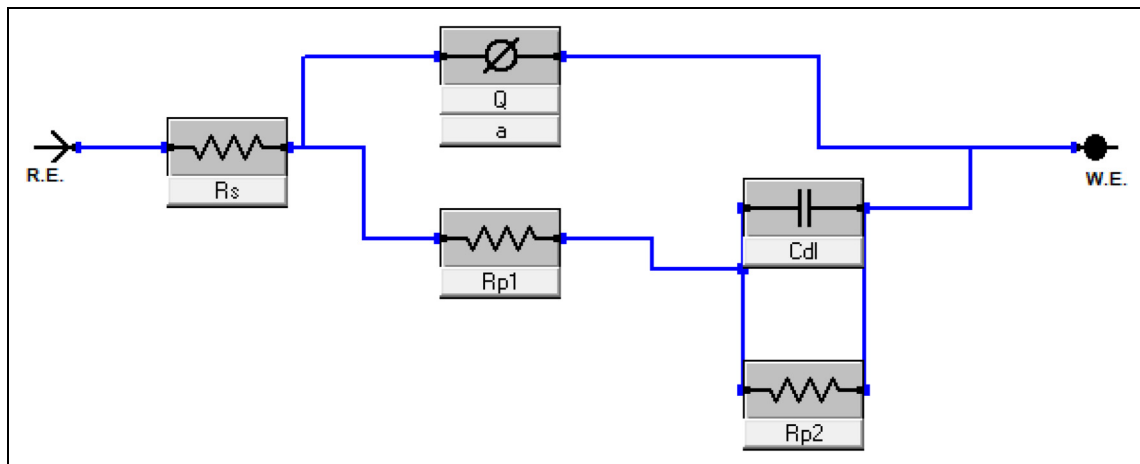

Figure 9. Open circuit potentials of composites as a function of time.

corrosion resistance due to the inert nature of NiTiB particles, the doped Al2024 samples still exhibit much higher corrosion resistance compared to the undoped Al2024 alloy.

Electrochemical impedance spectroscopy (EIS) was conducted to evaluate the corrosion resistance of the composites after stabilization in a 3.5% saline solution for 20 minutes, consistent with the results obtained from the potentiodynamic polarization tests and time-dependent open circuit potential measurements. The Nyquist curves obtained from EIS measurements, ranging from 100 kHz to 0. 2 Hz, are presented in Figure 11. These curves were fitted using the equivalent circuit shown in

Figure 12, and the fitting results are summarized in Table 6. In the equivalent circuit, Q represents the stationary phase element, Rp1 and Rp2 represent the primary and secondary polarization resistances, Cdl represents the double-layer capacitance, and Rs represents the solution resistance.

In the Nyquist curves, an increase in the semicircle diameter is associated with higher corrosion resistance. As depicted in Figure 11, the composite sample with 4% doping exhibits the highest corrosion resistance. Additionally, the values of a, which are close to 0.5, indicate that Q can also serve as an indicator of Warburg impedance. The upward trend of the Nyquist curves
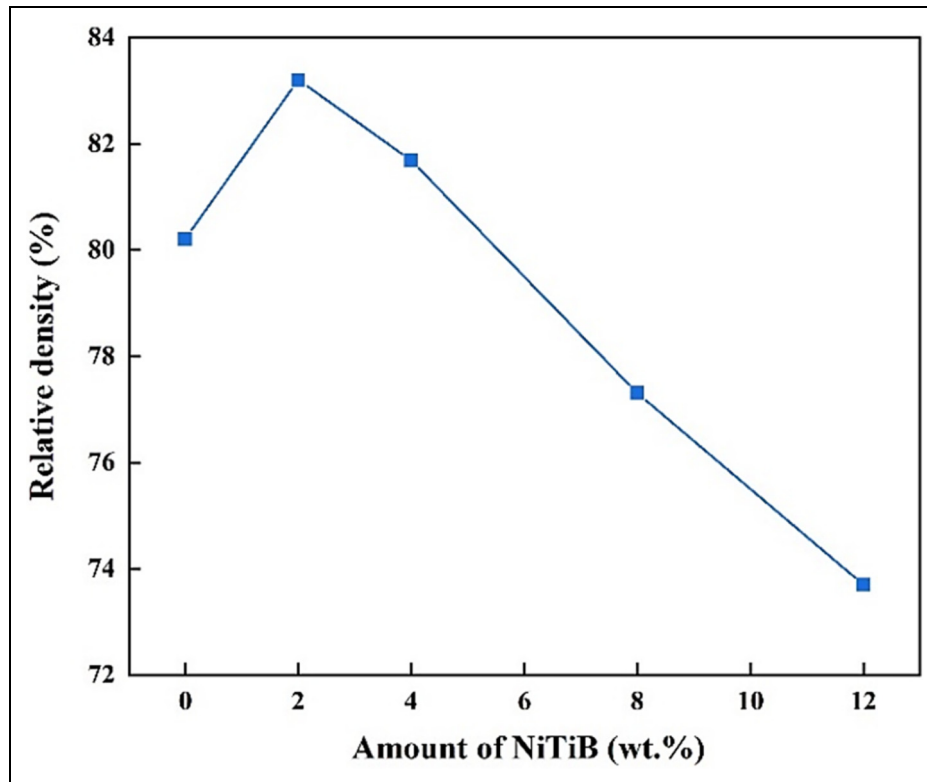
Figure 10. Potentiodynamic polarization curves of Al2024/NiTiB composites.

Table 5. Electrochemical parameters for polarization curves of the Al2024/NiTiB composites.

Sample	Ecorr (V)	icorr (μA/cm^2)	BetaA (V/decade)	BetaC (V/decade)	Corrosion Rate (mm/year)	Polarization Resistance (Rp)-Ω*cm^2)
Al2024	−1.128	88.44	460.5	277.9	0.936	8.51E + 05
Al2024 + %2 NiTiB	−1.054	15.079	515.7	197.4	0.199	4.11E + 06
Al2024 + %4 NiTiB	−0.722	3.345	374.4	181.4	0.042	1.59E + 07
Al2024 + %8 NiTiB	−0.927	5.592	270.6	226.7	0.067	9.58E + 06
Al2024 + %12 NiTiB	−0.953	11.425	397.2	177.6	0.130	4.66E + 06

further supports this finding. Warburg impedance reflects the passivation behavior on the composite surface.[43]

The composites with 4% and 8% doping display the highest total polarization resistance and corrosion resistance. This is consistent with the intersection of the potentiodynamic polarization curves and the open circuit potential, further confirming their superior corrosion resistance.

Abrasive wear behavior

The abrasive wear tests of Al2024 matrix-based composite samples reinforced with different proportions of nanocrystalline NiTiB particles were conducted using the pin-on-disk method on a 600 mesh abrasive paper with an applied load of 40 N. It is known that the wear losses increase or decrease depending on the size of the abrasive particles and the applied load. Since the main objective of this study is to investigate the effect of

NiTiB content in the composite structure on the wear behavior, the abrasive paper size and wear load were kept constant during the experiments. The experiments were conducted at a sliding velocity of 1.0 ms^{-1} and two different wear distances of 120 m and 240 m (Table 7). The graph in Figure 13 represents the wear loss values obtained from the abrasive wear tests.

Abrasive wear occurs when the material in contact with the abrasive surface is subjected to deformation due to the applied load and the resulting shearing force, leading to material removal.[43] In Figure 13, it is evident that the addition of NiTiB reinforcement significantly increases the abrasive wear resistance of the Al2024 composite. At a wear distance of 120 m, the wear amount for the pure Al2024 (0% reinforcement) reference sample is 0. 2297 g, whereas it is reduced to 0. 0938 g for the 2% NiTiB reinforced sample and further to 0. 0502 g for the 12% reinforced sample. This indicates a reduction in wear loss of 244% for the 2% NiTiB reinforcement and
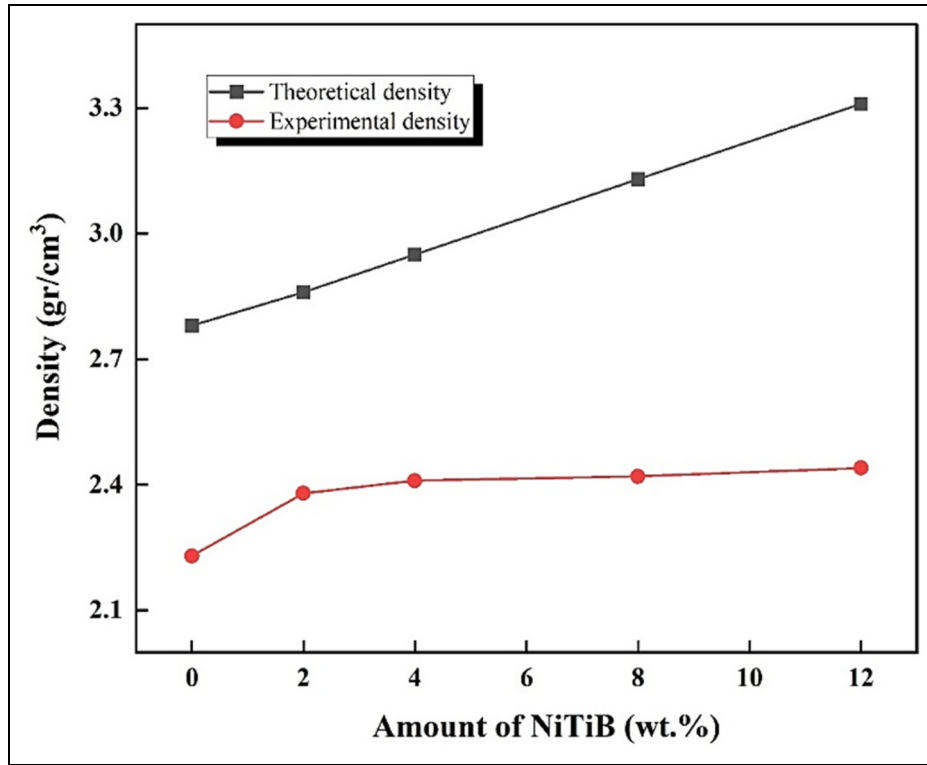
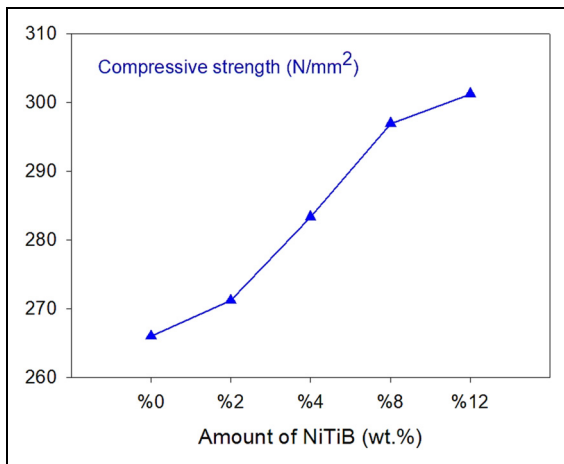**Figure 11.** Nyquist plots of Al2024/NiTiB composites.

Figure 12. The equivalent electrical circuit used for EIS tests.

Table 6. Equivalent circuit parameters for EIS of the Al2024/NiTiB composites.

Sample	Rs/Ω	Q/F.s^{a-1}	a	Rp1 + Rp2/ Ω	Cdl/F
Al2024	35.3	0.000255	0.595	1767	0.000658
Al2024 + %2 NiTiB	40.29	0.000240	0.773	3786	0.000163
Al2024 + %4 NiTiB	38.4	0.000144	0.663	5796	0.000005
Al2024 + %8 NiTiB	37.9	0.000095	0.740	4223	0.000432
Al2024 + % 12 NiTiB	36.54	0.000265	0.643	3856	0.000003

Table 7. Wear loss values of Al2024/NiTiB composites in grams.

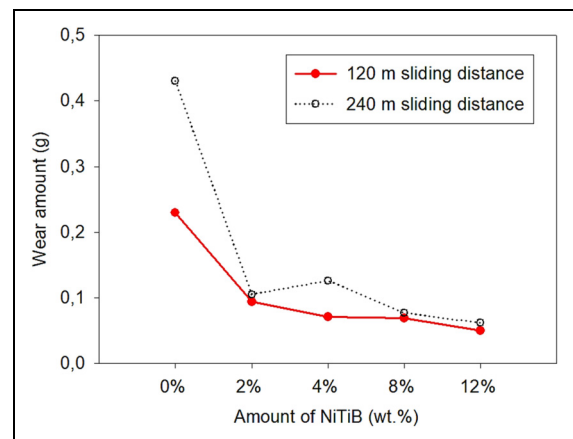| Sample	120 m Sliding distance	240 m Sliding distance
Al2024	0.2297	0.4302
Al2024 + %2 NiTiB	0.0938	0.1052
Al2024 + %4 NiTiB	0.0703	0.1260
Al2024 + %8 NiTiB	0.0687	0.0769
Al2024 + %12 NiTiB	0.0502	0.0614

Figure 13. Abrasive wear losses of Al2024/NiTiB nanocomposites containing different amounts of NiTiB.
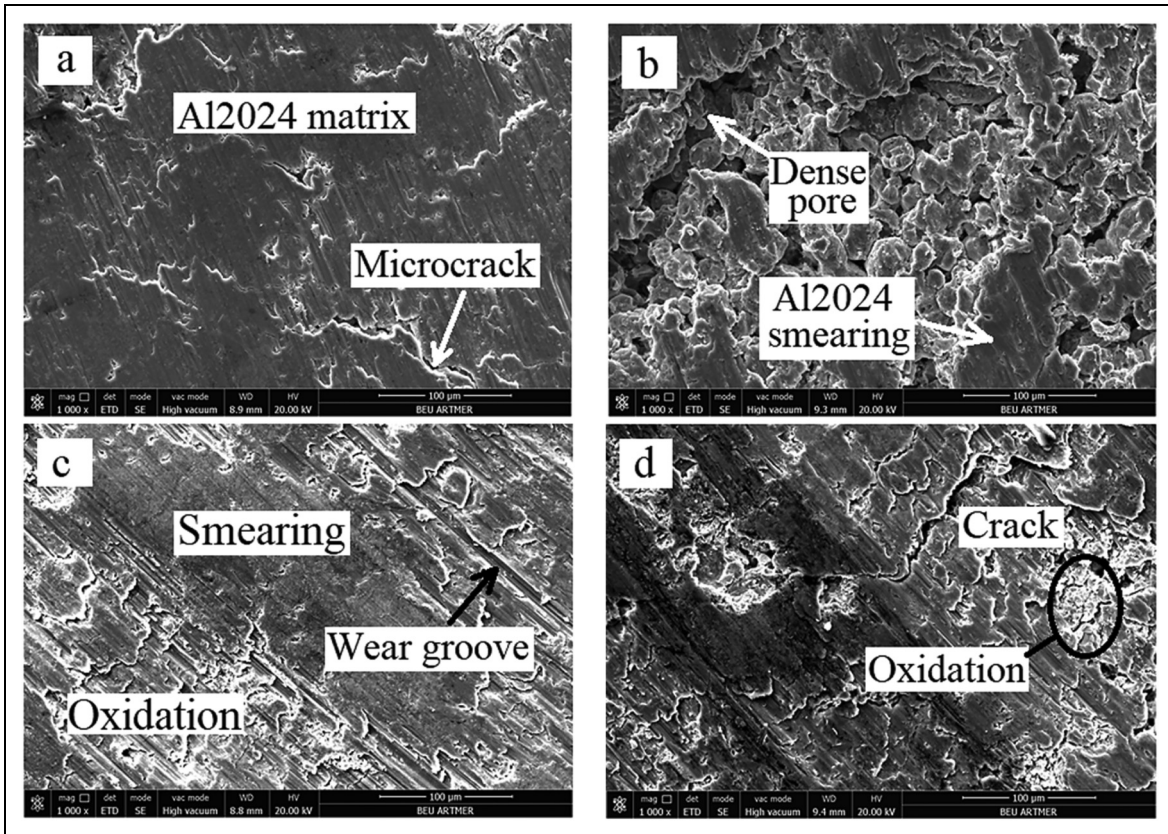
Figure 14. (a) Worn surfaces of Al2024/NiTiB composites reinforced with (a) 2% (b) 4%, (c) h 8%, (d) 12% NiTiB.
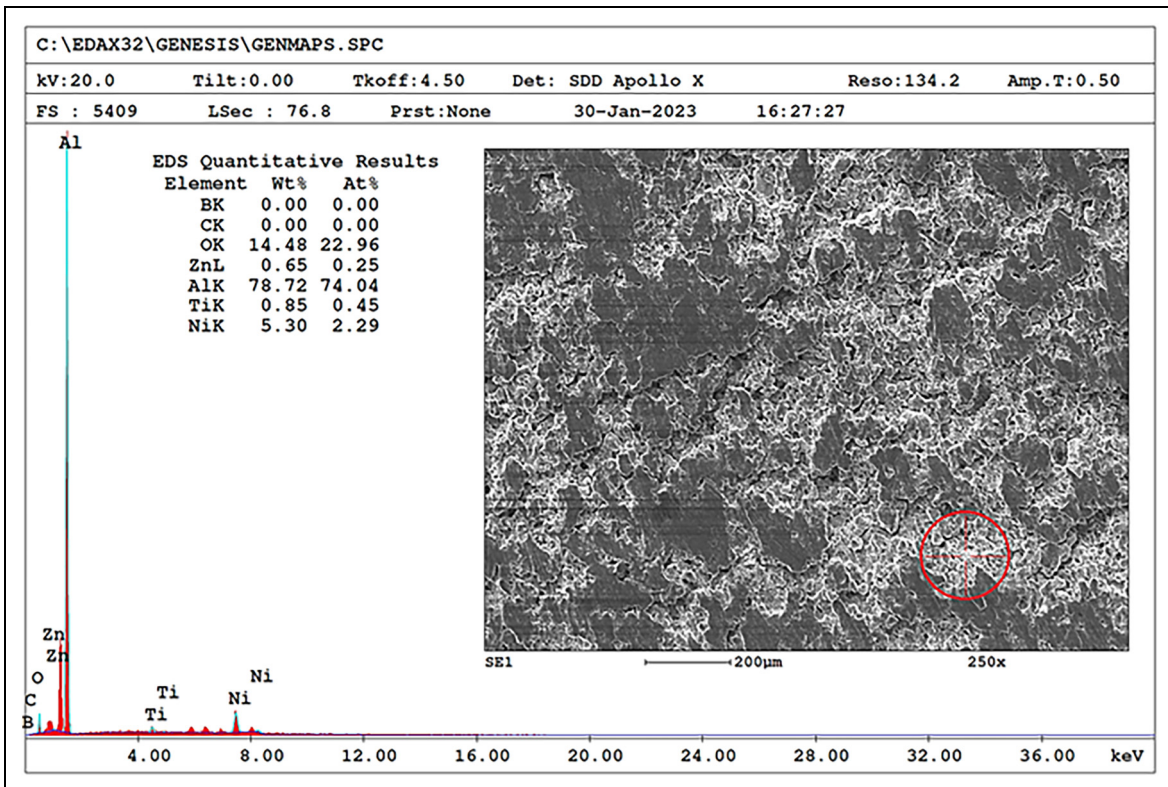

Figure 15. EDX analysis of the worn surface of the 4% NiTiB.

457% for the 12% NiTiB reinforcement samples. In particle-reinforced aluminum matrix composites, wear losses generally decrease depending on the physical properties of the reinforcement material, particularly its hardness. According to the Archard equation, the wear resistance of composites is directly related to their hardness (Equation (10)).

$$S = \mathrm{KWL} / H \qquad (10)$$

Here, Q represents the total wear volume, K is a dimensionless constant, W is the total normal load, L is the sliding distance, and H is the hardness of the softest contact surfaces. Similar studies have reported a positive effect of ceramic-based reinforcement elements used in MMCs on mechanical properties such as hardness.[44–46] It is generally observed that wear losses decrease as the reinforcement content of the hard phase in the matrix increases. Similar results have also been reported in various studies examining the wear of metal matrix composites reinforced with ceramic particles.[12,45,47–49] However, associating the wear resistance of composites solely with hardness is not sufficient, and the subject needs to be approached from different perspectives.[50] Abrasive wear is also related to the characteristics of the reinforcement element as well as the state of the phases formed within the composite structure.[51,52]

The obtained wear loss values in this experimental study appear to be quite successful compared to the literature. Particularly, the ceramic particles in the composite structure, which are harder than the matrix material, reduce the amount of wear. However, the success of wetting and bonding between the reinforcement particles and the matrix in the obtained composite structure indicates a direct relationship between the wear resistance of the composite and these factors. In the section evaluating the microstructures of the obtained composites, it was previously mentioned that the interfacial bonding between the matrix and the reinforcement was sufficient. The wear loss values in the abrasive wear tests also support this.

When examining Figure 13, it is evident that the wear losses of the NiTiB-reinforced composite specimens at a wear distance of 240 m do not follow the expected doubling trend observed in the pure Al2024 reference specimen. The discrepancy can be attributed to the elevated temperature between the specimen and abrasive surface due to the increased experimental duration and frictional effects during the wear tests.

As the duration of the experiment increases, the temperature rises, causing the Al2024 matrix material to soften. Some of the softened aluminum particles may remain in contact with the sandpaper surface and/or the specimen surface without detaching. These particles can then embed themselves into the scratches and pits formed on the specimen surface during the wear test. Consequently, these aluminum particles, which originally detached from the surface but reattached to it, can affect the accurate weight measurements conducted at the end of the experiment, resulting in lower-than-expected wear

loss values. To further investigate the wear behavior of the composite materials, SEM images were taken from the surfaces of the specimens that underwent wear testing at a distance of 240 m. These images are presented in Figure 14, providing visual evidence of the wear mechanisms and surface features.

Figure 14 shows characteristic features of abrasive wear, including wear tracks, surface deformations, micro and macro cracks, and voids. The abrasive SiC particles on the sandpaper act as cutting tools and exhibit a plowing effect on the sample surface during the abrasive wear experiments. This plowing effect can lead to localized accumulation of NiTiB reinforcement particles, resulting in the formation of porous regions where the SiC particles detach in bulk. This observation aligns with the unusual wear loss exhibited by the 4% NiTiB reinforced sample in the graph shown in Figure 13.

Furthermore, it should be noted that in this abrasive wear test, the primary abrasive agent is the sandpaper, while the NiTiB reinforcement particles in the composite also contribute to the wear process by detaching and scratching the surface, creating a secondary abrasive effect. As a result, the main wear mechanisms involved in the test can be identified as micro-cutting, micro-plowing, and micro-scratching, leading to plastic deformation of the material.[53]

Additionally, extensive oxidation can be observed on the surfaces of the composite samples as a result of the abrasive wear experiments being conducted in an open atmospheric environment. Aluminum is known to be highly susceptible to oxidation and undergoes rapid oxidation reactions. The friction generated during the experiments, followed by subsequent cooling, contributes to the occurrence of oxidation on the worn surfaces of the composite samples. To clarify this phenomenon, an EDX analysis of the worn surface of the 4% NiTiB-reinforced Al2024 composite is provided in Figure 15.

To further investigate this phenomenon, an EDX analysis of the worn surface of the 4% NiTiB-reinforced Al2024 composite is provided in Figure 15. This analysis enables the identification and mapping of the elemental composition on the surface. By examining the elemental distribution, potential insights into the oxidation process during abrasion, as well as the presence of various elements on the composite surface after abrasive wear, can be suggested.

Conclusions

The results obtained from this experimental study are summarized as follows:

1. NiTiB-reinforced Al2024 matrix composites were successfully produced using the powder metallurgy technique, with adequate wetting and bonding between the matrix material and nanocrystalline NiTiB particles.
2. Increasing the NiTiB content improved the homogeneity of the composite structure, but some

agglomerations and pore formations were observed to a minor extent.

3. The composite samples with 2% and 4% NiTiB doping exhibited the highest relative density and minimal porosity, resulting in improved mechanical properties.

4. Hardness tests showed that the 4% NiTiB reinforced composite had the highest hardness with an average of 80 HV among all specimens and loads, demonstrating the strengthening effect of the reinforcement particles.

5. Open circuit potential measurements indicated that the 4% NiTiB doped composite exhibited the highest corrosion resistance, while the undoped Al2024 sample showed the lowest corrosion potential.

6. Potentiodynamic polarization tests confirmed that the 4% doped composite had the highest corrosion potential and the lowest corrosion current density, indicating its superior corrosion resistance.

7. Electrochemical impedance spectroscopy tests supported the findings of the potentiodynamic polarization tests, with the 4% doped composite showing the highest polarization resistance.

8. NiTiB reinforcement resulted in increased hardness and compressive strength of the composites, demonstrating the strengthening effect of the reinforcement particles. The highest compressive strength of 301.2 N/mm^2 was measured from 12% NiTiB reinforced composite.

9. The addition of NiTiB reinforcement significantly improved the wear resistance of the composites, reducing wear losses compared to the pure Al2024 sample. The wear loss was reduced by 244% with 2% NiTiB reinforcement and 457% with 12% NiTiB reinforcement.

10. Increasing the wear distance did not lead to a proportional increase in wear losses, likely due to the softening of the Al2024 matrix material and the re-adhesion of detached particles during the wear test.

In conclusion, the addition of NiTiB reinforcement in the Al2024 matrix improved the mechanical and corrosion properties of the composites, while also enhancing wear resistance. The optimal reinforcement content was found to be 4%, which exhibited the highest corrosion resistance, hardness, and wear resistance among the tested compositions.

Data availability

The data that support the findings of this study are available from the corresponding author upon reasonable request.

Declaration of conflicting interests

The authors declared no potential conflicts of interest with respect to the research, authorship, and/or publication of this article.

ORCID iDs

Muharrem Pul [ID] https://orcid.org/0000-0002-0629-3516
Tuncay Şimşek [ID] https://orcid.org/0000-0002-4683-0152

References

1. Surappa MK. Aluminium matrix composites: challenges and opportunities. _Sadhana_ 2003; 28: 319–334.
2. Ujah CO and Kallon DVV. Trends in aluminium matrix composite development. _Cryst_ 2022; 12: 1357.
3. Srivastava A. Recent advances in metal matrix composites (MMCs): a review. _Biomed J Sci and Tech Res_ 2017; 1: 520–522.
4. Karaoglu SY, Karaoglu S and Unal I. Aerospace industry and aluminum metal matrix composites. _Ijast_ 2021; 2: 73–81.
5. Simsek T, Avar B, Ozcan S, et al. Solid-State synthesis and characterization of the stable nanostructured $Ni_{21}Ti_2B_6$ phase. _Phys Status Solidi B_ 2021; 258: 258.
6. Rondelli G, Vicentini B and Cigada A. The corrosion behaviour of nickel titanium shape memory alloys. _Corros Sci_ 1990; 30: 805–812.
7. Sinha AK. _Metals handbook, heat treating-boriding (boronizing) of steels_. USA: ASM International, Material Park, 1991, pp.978–999.
8. Srewart K. Boronizing protects metals against wear. _Adv Mater Process_ 1997; 3: 23–25.
9. Sidnov KP, Belov DS, Ponomareva AV, et al. Effect of alloying on elastic properties of ternary Ni-Al-Ti system: experimental validation. _Jalcom_ 2016; 688: 534–541.
10. Chen H, Zhang Z, Hao XH, et al. Microstructure and tribocorrosion properties of NiTi/AlNi$_2$Ti ternary intermetallic alloy. _Vacuum_ 2021; 184: 109928.
11. Zhao J, Zhao T, Zhang Y, et al. Corrosion behavior of the 2024 aluminum alloy in the atmospheric environment of the South China Sea Islands. _Coatings_ 2024; 14: 331.
12. Reddy PS, Kesavan R and Ramnath BV. Evaluation of mechanical properties of aluminum alloy (Al2024) reinforced with silicon carbide (SiC) metal matrix composites. _Solid State Phenom_ 2017; 263: 184–188.
13. Doğan H and Mutlu Y. Production of AA2024-matrix B_4C-SiC- and B_4C-Y_2O_3-particle-reinforced composites by powder metallurgy and investigation of their mechanical properties. _CBU J Sci_ 2022; 18: 321–330.
14. Murthy IN, Babu NA and Rao JB. Comparative studies on microstructure and mechanical properties of granulated blast furnace slag and fly ash reinforced AA 2024 composites. _J Met Mater Miner_ 2014; 2: 319–333.
15. Rebba B and Ramanaiah N. Evaluation of mechanical properties of aluminium alloy (Al-2024) reinforced with molybdenum disulphide (MOS2) metal matrix composites. _Procedia Mater Sci_ 2014; 6: 1161–1169.
16. Dey D and Biswas A. Comparative study of physical, mechanical and tribological properties of Al2024 alloy and SiC-TiB$_2$ composites. _Silicon_ 2021; 13: 1895–1906.
17. Nuruzzaman DM, Kamaruzaman FFB and Azmi NBM. Effect of sintering temperature on the properties of aluminium-aluminium oxide composite materials. _IJEMM_ 2016; 1: 59–64.

18. Luoa ZP and Sun CY. Effect of the interfacial bonding status on the tensile fracture characteristics of a boron–fiber-reinforced aluminum composite. *Mater Charact* 2003; 50: 51–58.

19. Heidarpour A, Mousavi ZS, Karimi S, et al. On the corrosion behavior and microstructural characterization of Al2024 and Al2024/Ti2SC MAX phase surface composite through friction stir processing. *J Appl Electrochem* 2021; 51: 1123–1136.

20. Kumar P, Parhi S and Datta S. Comparative study of Al-TiB$_2$ composite fabricated by different powder metallurgical methods. *Int J Emerg Res Manag Technol* 2017; 6: 178–187.

21. Pul M. The effect on mechanical properties of reinforcement amount at B42 C+ TiB reinforced Al 2024 based composites produced by powder metallurgy. *Int J Eng Res. Dev* 2019; 11: 87–99.

22. Bharathi P and Kumar PS. Mechanical characteristics and wear behaviour of Al/SiC and Al/SiC/ B$_4$C hybrid metal matrix composites fabricated through powder metallurgy route. *Silicon* 2023; 15: 4259–4275.

23. Manoj M, Jinu GR, Kumar JS, et al. Effect of TiB2 particles on the morphological, mechanical and corrosion behaviour of Al7075 metal matrix composite produced using stir casting process. *Int J Met* 2021; 16: 1517–1532.

24. Astm G. Standard Practice for Calculation of Corrosion Rates and Related Information from Electrochemical Measurements, 102-89(2015)e1.

25. Nelson EE. Discussion of the mechanism of passivating-type inhibitors. *J Electrochem Soc* 1959; 106: 638–664.

26. Suryanarayana C. Mechanical alloying: a critical review. *Materials Research Letters* 2022; 10: 619–647.

27. Suryanarayana C. Mechanical alloying and milling. *Prog Mater Sci* 2001; 46: 1–184.

28. Pul M. Effect of sintering on mechanical property of SiC/B$_4$C reinforced aluminum. *Mater Res Express* 2019; 6: 016541.

29. Lillo TM. Enhancing ductility of Al6061+ 10 wt% B$_4$Cthrough equal-channel angular extrusion processing. *Mater Sci Eng A* 2005; 410: 443–446.

30. Salvador MD, Amigo V, Martinez N, et al. Development of Al–Si–Mg alloys reinforced with diboride particles. *J Mater Process Tech* 2003; 143: 598–604.

31. Mandal A, Chakraborty M and Murty BS. Ageing behaviour of A356 alloy reinforced with in-situ formed TiB2 particles. *Mater Sci Eng A* 2008; 489: 220–226.

32. Saboori A, Moheimani SK, Dadkhah M, et al. An overview of key challenges in the fabrication of metal matrix nanocomposites reinforced by graphene nanoplatelets. *Metals (Basel)* 2018; 8: 172.

33. Rahimian M, Parvin N and Ehsani N. Investigation of particle size and amount of alumina on microstructure and mechanical properties of Al matrix composite made by powder metallurgy. *Mater Sci Eng A* 2010; 527: 1031–1038.

34. Hosseini Vajargah P, Abdizadeh H and Baghchesara MA. Fabrication of TiB$_2$ nanoparticulates reinforced aluminum matrix composites by powder metallurgy route. *J Compos Mater* 2015; 49: 3115–3125.

35. Aydın F. Investigation of elevated temperature wear behavior of Al 2024-BN composites using statistical techniques. *J Mater Eng Perform* 2021; 30: 8560–8578.

36. Pul M. Effect of B$_4$C reinforcement ratio and sintering temperature on the mechanical behavior in Al-B$_4$C composites. *Sci Sinter* 2018; 50: 51–61.

37. Duan X, Han T, Guan X, et al. Cooperative effect of Cr and Al elements on passivation enhancement of eutectic high-entropy alloy AlCoCrFeNi2.1 with precipitates. *J Mater Sci Technol* 2023; 136: 97–108.

38. Zhang LW, Xu JL, Chen J, et al. Microstructure and corrosion resistance of AlCoCrFeNi high-entropy alloy coating on sintered NdFeB magnets prepared by HVOF spraying. *J Magn Magn Mater* 2022; 551: 169136.

39. Sherif ESM, Abdo HS, Khalil KA, et al. Effect of titanium carbide content on the corrosion behavior of Al-TiC composites processed by high energy ball mill. *Int J Electrochem Sci* 2016; 11: 4632–4464.

40. Wang ZG, Li CP, Wang HY, et al. Wear and corrosion behavior of functionally graded nano-SiC/2014Al composites produced by powder metallurgy. *J Mater Eng Perform* 2017; 26: 729–735.

41. Poria S, Sutradhar G and Sahoo P. Corrosion behavior of stir-cast Al–TiB$_2$ metal matrix composites. *Int J Mater Res* 2019; 110: 148–154.

42. Kumar PS, Kavimani V, Prakash KS, et al. Effect of TiB$_2$ on the corrosion resistance behavior of in situ Al composites. *Int J Met* 2020; 14: 84–91.

43. Ammar R, Sherif EM, Sivasankaran S, et al. Developing improved corrosion-resistant AA5083—BN/WC composites for tribological applications. *Materials (Basel)* 2023; 16: 1663.

44. Hasirci H and Gul F. Investigation of abrasive wear behaviors in B$_4$C/Al composites depending on reinforcement volume fraction. *SDU Int Technol Sci* 2010; 2: 15–21.

45. Abenojar J, Velasco F and Martinez MA. Optimization of processing parameters for the Al+ 10% B$_4$C system obtained by mechanical alloying. *J Mater Process Technol* 2007; 184: 441–446.

46. Sun Y, Baydogan M and Cimenoglu H. The effect of deformation before ageing on the wear resistance of an aluminum alloy. *Mater Lett* 1999; 38: 221–226.

47. Ramachandra M, Abhishek A, Siddeshwar P, et al. Hardness and wear resistance of ZrO$_2$ nano particle reinforced Al nanocomposites produced by powder metallurgy. *Proc Mat Sci* 2015; 10: 212–219.

48. Pandiyarajan R, Maran P, Marimuthu S, et al. Mechanical and tribological behavior of the metal matrix composite AA6061/ZrO$_2$/C. *J Mech Sci Technol* 2017; 31: 4711–4717.

49. Yilmaz O and Buytoz S. Abrasive wear of Al$_2$O$_3$- reinforced aluminum-based MMCs. *Compos Sci Technol* 2001; 61: 2381–2392.

50. Jiang QC, Xu CL, Lu M, et al. Effect of new Al–P–Ti–TiC–Y modifier on primary silicon in hypereutectic Al–Si alloys. *Mater Lett* 2005; 59: 624–628.

51. Candan E, Ahlatci H and Cimenoglu H. Abrasive wear behaviour of Al–SiC composites produced by pressure infiltration technique. *Wear* 2001; 247: 133–138.

52. Berger M, Wiklund U, Eriksson M, et al. The multilayer effect in abrasion–optimising the combination of hard and tough phases. *Surf Coat Technol* 1999; 116: 1138–1144.

53. Pul M. The effect of B4C and GNP reinforcement amounts on abrasive wear behavior in Al 6061/B4C/GNP hybrid composites. *NOHU J Eng Sci* 2022; 11: 1179–1187.